Topology Optimization of Asymmetric PMSM Rotor

Théodore Cherrière, S Hlioui, Luc Laurent, François Louf, Hamid Ben Ahmed, Mohamed Gabsi

Topology Optimization of Asymmetric PMSM Rotor

T. Cherrière, S. Hlioui, *Member, IEEE*, L. Laurent, F. Louf, H. Ben Ahmed, and M. Gabsi

***Abstract*—This paper investigates the optimization of iron distribution in the rotor of a permanent magnet synchronous machine. The objective is to maximize the average torque for fixed permanent magnets positions, stator, and current feedings. To do so, a density-based algorithm is used with the adjoint variable method to compute sensitivities. It returns non-symmetric geometries, which are related to the interactions between magnets and winding fluxes, as well as the machine operating mode (motor or generator for a given rotation direction). For a given single working point, we obtain asymmetric topologies that outperform the optimized symmetric design, while the symmetric rotor topology is more multifunctional.**

***Index Terms*—Asymmetric rotor, Density method, Nonlinear magnetostatics, PM machine, Topology optimization**

I. Introduction

Topology optimization of electrical machines is a fast-growing research field. Since [1], numerous approaches have emerged, such as the level-set method based on shape derivative [2] or topological derivative [3], or the phase-field method [4] (see [5] for an overview). The most popular ones are based on density approaches, derived from [6].

In the field of electrical machines, these density-based methodologies are widely used mainly for the optimization of reluctance machines [7], but also for multi-material optimization [8], that can include multiphysics [9]. Permanent magnets can also be included in the optimization process with a hybrid method [10] or directly with auxiliary variables [11]. These methodologies aim to solve the following standard optimization problem:

$$\begin{aligned} &\text{find} && \boldsymbol{\rho}_{\text{opt}} = \arg\min_{\boldsymbol{\rho}\in\mathbb{R}^N} f(\boldsymbol{\rho}), \\ &\text{subjected to} && \begin{cases} g_i(\boldsymbol{\rho}) = 0 & \forall i \in [\![1, n_g]\!] \\ h_j(\boldsymbol{\rho}) \leq 0 & \forall j \in [\![1, n_h]\!], \end{cases} \end{aligned} \tag{1}$$

where $\boldsymbol{\rho}$ is the vector of optimization variables, f the objective function to minimize, g_i the equality constraints and h_j the inequality constraints. In topology optimization problems, the number of optimization variables N is large, *i.e.* $N > 10^3$. Gradient-based algorithms are then preferred to heuristic ones because they require less computational effort, even if they may provide local optima [12]. The most popular optimization algorithms include the method of moving asymptotes [13], optimality criteria (for compliance type problems) [14] and sequential linear programming [7].

Within this formalism, the shape is described by an element-based pixelated representation as in Fig. 1. In the solid/void case, each value of $\boldsymbol{\rho}$ corresponds to the density of a fixed grid element: 0 when it is filled with air, and 1 when it is filled with solid material such as iron. There are always at least two inequality constraints per pixel associated with these lower and upper bounds of the density.

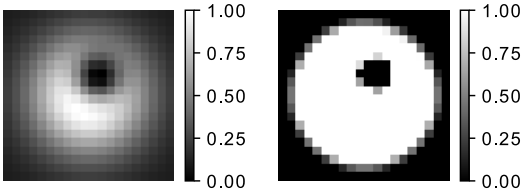

Fig. 1. Density-based geometry representations. The design is pixelated, possibly containing intermediate materials (grey).

To be interpreted as a proper geometry, $\boldsymbol{\rho}_{\text{opt}}$ is discrete and should be in $\{0,1\}^N$. To compute the problem sensitivities, the material properties are $\mathcal{C}^1$ - interpolated on $\boldsymbol{\rho}$ during the optimization process. Consequently, non-physical intermediate materials with densities between 0 and 1 exists. They should be eliminated as much as possible at the end of the optimization process. In mechanical engineering, a mass constraint (the weighted sum of all components of $\boldsymbol{\rho}$) associated with a penalization on the interpolation [15] allows the optimizer to eliminate intermediate materials efficiently. Other difficulties could be due to the mathematical definition of the optimization problem, which may be ill-posed and lead to mesh dependency, or to numerical discretization (such as checkerboard artifacts). It is usually solved with filtering or by additional constraints [16].

This work investigates a density-based topology optimization of the iron distribution within a Permanent Magnet Synchronous Machine (PMSM) rotor considering different working points. The objective is to maximize the average torque for fixed stator, current feeds, and Permanent Magnets (PM) positions. This paper is organized as follows. The problem is defined and the implementation is detailed in Section II. Next, the methodology is applied to three different operating modes: pure motor (Section III-B), pure generator (Section III-C) and mixed motor/generator (Section III-D). The results are then discussed and analyzed in Section IV, focusing on the symmetry of the obtained designs, which open up future perspectives identified in Section V.

T. Cherrière and M. Gabsi are with SATIE laboratory, ENS Paris-Saclay, CNRS, Paris-Saclay University, 91190, Gif-sur-Yvette, France (e-mail: theodore.cherriere@ens-paris-saclay.fr).

S. Hlioui is with SATIE Laboratory, CY Cergy Paris University, CNRS, Paris-Saclay University, 95000 Cergy, France.

L. Laurent is with Laboratoire de Mécanique des Structures et des Systèmes Couplés, Conservatoire national des arts et métiers, Case 2D6R10, 2 rue Conté , 75003 Paris, France and HESAM University, Paris, France.

F. Louf is with LMPS - Laboratoire de Mécanique Paris-Saclay, CentraleSupélec, ENS Paris-Saclay, CNRS, 91190, Gif-sur-Yvette, Paris-Saclay University, France.

H. Ben Ahmed is with SATIE Laboratory, ENS Rennes, CNRS, 35170 Bruz, France.

II. Problem definition

A. 2D magnetostatics

Although there are several possibilities to set a magnetostatic problem, the most popular approach chosen in topology optimization is the $\boldsymbol{a}$–formulation, based on the magnetic vector potential $\boldsymbol{a}$. The static Maxwell equations lead to the following magnetostatics local "strong" equation:

$$\nabla \times (\overline{\overline{\nu}}.\nabla \times \boldsymbol{a}) = \boldsymbol{j} + \nabla \times \boldsymbol{m}, \tag{2}$$

with $\boldsymbol{j}$ the current density, $\overline{\overline{\nu}}$ the reluctivity tensor and $\boldsymbol{m}$ the magnetization of permanent magnets. For isotropic problems, $\overline{\overline{\nu}}$ is scalar denoted by ν. Usually, the magnetic domain contains nonlinear ferromagnetic materials, so ν depends on the flux density norm $\boldsymbol{b} = \nabla \times \boldsymbol{a}$. In two-dimensional problems, the x and y components of $\boldsymbol{a}$ and $\boldsymbol{j}$ vanish as well as the z component of $\boldsymbol{m}$. Under these assumptions, Eq. (2) becomes:

$$\nabla.(\nu(a_z).\nabla a_z) = j_z + \nabla \left(\begin{bmatrix} 0 & 1 \\ -1 & 0 \end{bmatrix} \boldsymbol{m} \right). \tag{3}$$

This local equation can be discretized using for instance the Finite Element Method (FEM), and gives the following nonlinear system:

$$\mathbf{K}(\nu(\mathbf{a}))\mathbf{a} = \mathbf{s}, \tag{4}$$

where $\mathbf{K}$ is called the stiffness matrix, $\mathbf{a}$ is the degrees of freedom vector, and $\boldsymbol{s}$ is the right-hand side related to the source terms. $\mathbf{K}$ depends on ν, which depends itself on the local flux density and material behavior. The Newton-Raphson method is used to solve the nonlinear system (4). It minimizes the residual $\boldsymbol{r}_n = \mathbf{K}_n\mathbf{a}_n - \mathbf{s}$ by applying the following iterative procedure until convergence:

$$\mathbf{a}_{n+1} = -\left(\frac{\mathrm{d}\boldsymbol{r}_n}{\mathrm{d}\mathbf{a}} \right)^{-1} \boldsymbol{r}_n + \mathbf{a}_n. \tag{5}$$

The tangent operator reads [5]:

$$\left(\frac{\mathrm{d}\boldsymbol{r}_n}{\mathrm{d}\mathbf{a}} \right)_{ij} = (\mathbf{K}_n)_{ij} + \sum_k \frac{\mathrm{d}(\mathbf{K}_n)_{ik}}{\mathrm{d}a_j} \mathrm{a}_k. \tag{6}$$

B. Adjoint Variable Method (AVM)

The AVM is the most efficient way to compute the gradient of an objective function f which depends implicitly on a large number of variables through a system like (4) [17]. Its computation time compared with the non-linear FEM is given in Fig. 8. Let us consider $f : \boldsymbol{\rho} \mapsto f(\boldsymbol{\rho}, \mathbf{a}(\boldsymbol{\rho}))$ and we want to calculate $\nabla_{\boldsymbol{\rho}} f$. The chain rule reads for each component ρ_i:

$$\frac{\mathrm{d}f}{\mathrm{d}\rho_i} = \frac{\partial f}{\partial \rho_i} + \left(\frac{\partial f}{\partial \mathbf{a}} \right)^T \cdot \frac{\mathrm{d}\mathbf{a}}{\mathrm{d}\rho_i}. \tag{7}$$

The term $\frac{\partial f}{\partial \rho_i}$ is zero when the dependence of the objective function with the density is not explicit, which is often the case. The difficulty arises from the absence of an explicit expression for $\frac{\mathrm{d}\mathbf{a}}{\mathrm{d}\rho_i}$. By derivating the residual of (4), we obtain the following linear system:

$$\frac{\partial \boldsymbol{r}}{\partial \mathbf{a}} \frac{\mathrm{d}\mathbf{a}}{\mathrm{d}\rho_i} = -\frac{\partial \mathbf{K}}{\partial \rho_i}\mathbf{a}, \tag{8}$$

and by introducing the so-called *adjoint system*:

$$\left(\frac{\partial \boldsymbol{r}}{\partial \mathbf{a}} \right)^T \boldsymbol{\lambda} = \frac{\partial f}{\partial \mathbf{a}}, \tag{9}$$

one can rewrite the implicit part of (7) as:

$$\left(\frac{\partial f}{\partial \mathbf{a}} \right)^T \frac{\mathrm{d}\mathbf{a}}{\mathrm{d}\rho_i} = \underbrace{\left(\frac{\partial f}{\partial \mathbf{a}} \right)^T \left(\frac{\partial \boldsymbol{r}}{\partial \mathbf{a}} \right)^{-1}}_{(9)^T} \underbrace{\frac{\partial \boldsymbol{r}}{\partial \mathbf{a}} \frac{\mathrm{d}\mathbf{a}}{\mathrm{d}\rho_i}}_{(8)} = -\boldsymbol{\lambda}^T \frac{\partial \mathbf{K}}{\partial \rho_i}\mathbf{a}. \tag{10}$$

The three terms of Eq. (10) are:

- The direct state $\mathbf{a}$ is the solution of the physical problem (4) . Its resolution also gives the tangent operator $\frac{\partial \boldsymbol{r}}{\partial \mathbf{a}}$.
- The adjoint state $\boldsymbol{\lambda}$ is the solution of the linear system (9) , which needs to be solved only once.
- The stiffness matrix derivative $\frac{\partial \mathbf{K}}{\partial \rho_i}$ depends explicitly on the material interpolation, detailed hereafter.

C. Material interpolation

Two choices are reported on the interpolation of the magnetic properties in the literature:

- Historically, magnetic permeability $\mu = \nu^{-1}$ has been used since [1].
- The magnetic reluctivity ν is the other alternative, introduced in [18] where it seems to perform better for simple problems.

In this paper, we choose a linear interpolation on the reluctivity because it guarantees a physical magnetic behavior for intermediate materials:

$$\nu_k(\rho_i, |\boldsymbol{b}|) = \nu_0 + \rho_i(\nu_{\text{iron}}(|\boldsymbol{b}|) - \nu_0), \tag{11}$$

where ρ_i is the density associated with the mesh element i. The expression (11) is used in (10) to evaluate $\frac{\partial \mathbf{K}}{\partial \rho_i}$. This interpolation can be rewritten as:

$$\nu_k(\rho_i, |\boldsymbol{b}|) = \underbrace{(1-\rho_i)}_{\Lambda_{\text{air}}} \nu_0 + \underbrace{\rho_i}_{\Lambda_{\text{iron}}} \nu_{\text{iron}}(|\boldsymbol{b}|). \tag{12}$$

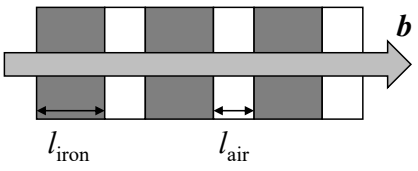

Fig. 2. Serial assembly of magnetic materials.

The expression (12) is the homogenized magnetic reluctivity of a serial assembly of magnetic materials along the flux lines: $\Lambda_{\text{air}} = \frac{l_{\text{air}}}{l_{\text{air}}+l_{\text{iron}}}$ and $\Lambda_{\text{iron}} = \frac{l_{\text{iron}}}{l_{\text{air}}+l_{\text{iron}}}$ are the

lineic fractions of air and iron, respectively, as shown in Fig. 2. Under these conditions, the BH curves of intermediate materials are plotted in Fig. 3.

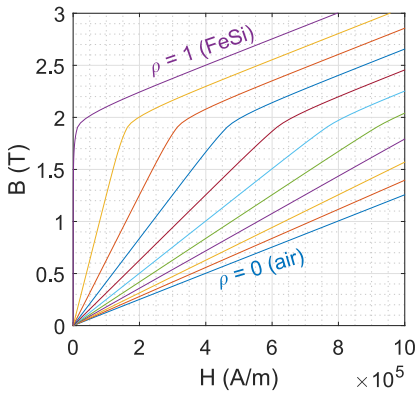

Fig. 3. Magnetic behavior of intermediate materials interpolated by (11) for all ρ values linearly spaced from 0 (air) to 1 (FeSi) with a step of 0.1.

D. Implementation

We implemented the topology optimization framework and the magnetostatic solver in MATLAB. The FEM solver uses first-order triangular elements. The Newton-Raphson algorithm with load ramping evaluates the direct state $\mathbf{a}$ from (4). This solver was compared with GetDp [19] and validated.

The objective function f is the average torque computed with Arkkio's method [20] on 60 positions along one magnetic pole. The rotation is implemented with a locked-step sliding band approach [21] to avoid remeshing and save computational time between each angular position.

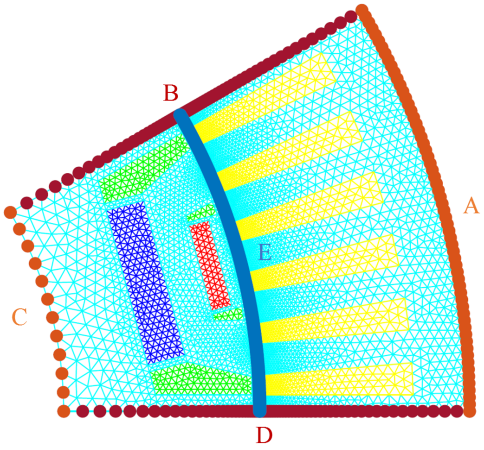

Fig. 4. Mesh generated with GMSH [22] (11331 triangles, 5890 nodes). Dirichlet boundary condition is imposed on A and C, antiperiodicity (master/slave) is imposed on B and D, and a sliding band emulates the rotation between the rotor and the stator on E.

It is unnecessary to impose a mass constraint on this problem. In contrast to mechanical engineering, a full solid design is not optimal to maximize the torque because it cancels the reluctant torque and introduces magnetic short circuits, decreasing the hybrid torque. Therefore, neither filtering nor penalization process was implemented in this paper. We apply a simple descent algorithm with projected box-constraints on $\boldsymbol{\rho}$. The following expression gives the descent direction $\boldsymbol{d}$ to accelerate the convergence. It involves the sensitivities (10) evaluated with the AVM:

$$\boldsymbol{d} = -\text{sign}\left(\nabla_{\boldsymbol{\rho}} f\right). \tag{13}$$

A trust-region-like algorithm controls the step size [23]. It compares the expected variation of objective function $\Delta_{\text{exp}} f$ obtained from $\nabla_{\boldsymbol{\rho}} f$ with the real one Δf. It increases the step if $\frac{\Delta_{\text{exp}} f}{\Delta f} > c > 0$, or rejects the iteration and decreases the step size otherwise. The tolerance is chosen as $c = 10^{-2}$. The algorithm stops when the step size α is small enough ($\alpha_{\min} = 10^{-3}$), or when it reaches the maximum number of iterations $n_{\max} = 500$. The flowchart is plotted in Fig. 5.

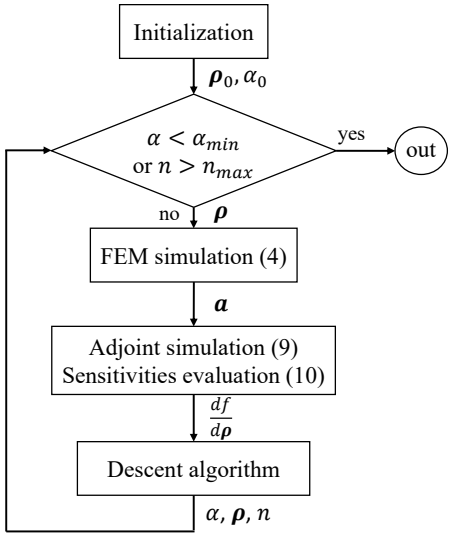

Fig. 5. Flowchart of the optimization algorithm.

III. Application on a PMSM Rotor

A. Presentation of the test cases

We apply this methodology to optimize the iron distribution within a PMSM rotor to maximize the average torque for a given stator shape and current density. The PM positions are fixed as in the simplified rotor of the BMW i3 [24] shown in Fig. 6. All results are given for a normalized axial length $L = 1\,\text{m}$. The iron magnetic behavior is similar to traditional FeSi plotted on Fig. 3 for $\rho = 1$. The PM are assumed ideal (constant magnetization, with a remanent flux density $B_r = 1\,\text{T}$ and a permeability μ_0). The current densities of the three phases depend on the electrical angle θ_e and read:

$$\begin{cases} J_A(\theta_e) = J\cos\left(\theta_e + \phi\right) \\ J_B(\theta_e) = J\cos\left(\theta_e - \frac{2\pi}{3} + \phi\right) \\ J_C(\theta_e) = J\cos\left(\theta_e + \frac{2\pi}{3} + \phi\right), \end{cases} \tag{14}$$

where the current density amplitude J is set as $10\,\text{A}/\text{mm}^2$. The load angle ϕ represents an angular displacement between the rotor and the magnetic flux created by the stator. It plays

an essential role in the optimization process and should be carefully chosen depending on the working point. The initial rotor shown in Fig. 7 is, in fact, not rotationally invariant as it contains fixed PM.

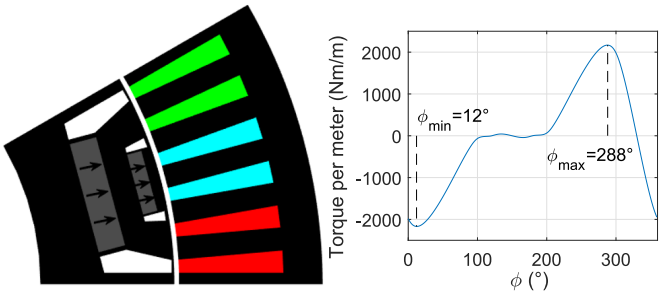

(a) Reference design (b) Average torque with load angle

Fig. 6. Reference design with associated performance. The materials and conductors legend is given in Fig. 7.

The reference design (Fig. 6a) allows the computation of the minimum torque load angle $\phi_{\text{min}} = 12°$, as well as the maximum torque load angle $\phi_{\text{max}} = 288°$ (Fig. 6b). Then, three test-cases are studied:

- **Pure motor**: maximization of the average motor torque $\langle C_m \rangle$ with $\phi = \phi_{\text{max}}$ – see section III-B.
- **Pure generator**: minimization of the average generator torque $\langle C_g \rangle$ with $\phi = \phi_{\text{min}}$ – see section III-C.
- **Reversible case**: maximization of the objective function $\langle C_r \rangle = (\langle C_m \rangle - \langle C_g \rangle)/2$ – see section III-D.

The initial situation is represented in Fig. 7, with an intermediate density $\rho = 0.5$ everywhere in the rotor except where the PM are located. The stator is imposed so that both the magnetic flux and the rotor spin synchronously in the trigonometric direction. However, by contrast with [25] where a similar problem is adressed, there is no constraint on the symmetry of the rotor.

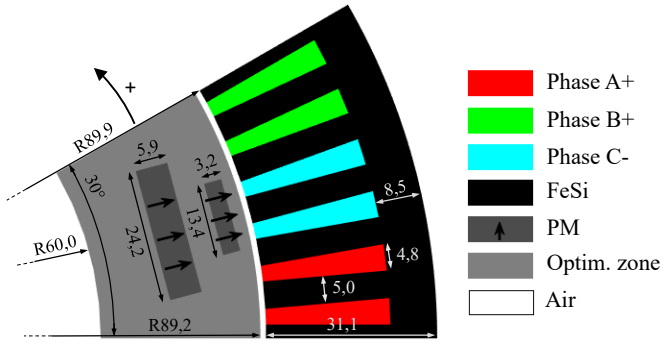

Fig. 7. Initial situation. The stator and PM are fixed and are not part of the optimization. The dimensions are given in millimeters, *R* indicates a radius.

Table I summarizes the final torque results. The torque history, the gradient norm, and the step size at each accepted iteration of the optimization process are also given to show the convergence. In all optimizations, the minimum step size $\alpha_{\text{min}} = 10^{-3}$ was reached before the maximum number of iterations n_{max} set at 500.

Fig. 8 shows the computing time statistics for one standard optimizer iteration, which contains the FEM and the AVM analyses on 60 rotor positions. Note that in a reversible case, this time is doubled because both the motor and the generator working points are computed. The variability of the non-linear FEM computing time is high because the number of Newton-Raphson iterations (5) depends strongly on the geometry and the saturation level.

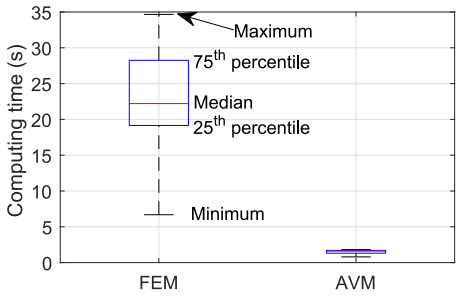

Fig. 8. Single-thread computing time per iteration of the optimization algorithm (AMD Threadripper 3975WX 3.5 GHz - 64 Go of RAM). The FEM average computing time is 23 s while the AVM one is 1.5 s.

B. Motor operating mode

First, we process the optimization for a motor working point. The optimization leads to an asymmetric iron distribution shown in Fig. 9a. Its average torque is $2554\,\text{Nm/m}$, which is better than the reference design ($2169\,\text{Nm/m}$) and the optimized symmetric design presented in section III-D ($2497\,\text{Nm/m}$ for this particular working point). This asymmetry is not conventional since electrical machine engineers generally propose symmetric designs for this situation. An interpretation of the result is presented in section IV.

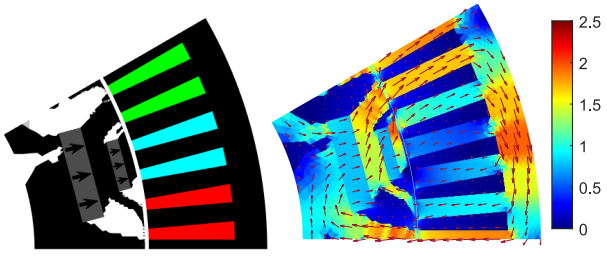

(a) Final design ($B_r = 1\,\text{T}$) (b) Associated flux density (T)

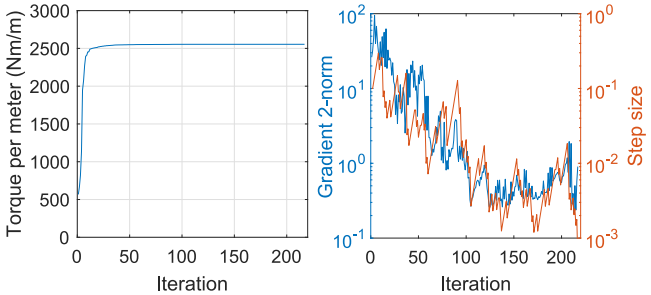

(c) Average torque during the optimization process (d) Gradient norm and step size during the optimization process

Fig. 9. Optimization results for a motor working point.

C. Generator operating mode

The reversed asymmetry appears again when changing the working point from motor to generator, as shown in Fig. 10. It returns the inverted motor structure from section III-B, which could also be interpreted as the same machine with a reverse rotation direction. This means that there is a preferred rotation direction for asymmetric designs depending on the operating mode, as shown in Tables I and II.

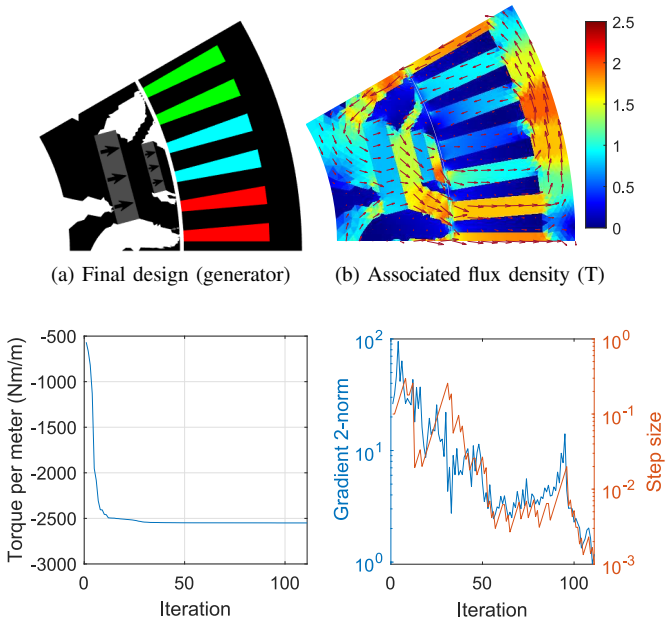

(a) Final design (generator) (b) Associated flux density (T)

(c) Average torque during the optimization process (d) Gradient norm and step size during the optimization process

Fig. 10. Optimization results for a generator working point.

D. Reversible mode

The results of previous optimizations have shown that:

- The working point of the machine has a significant impact on the rotor asymmetry.
- The motor and generator structures are mirrors of each other, so they can be interpreted as the same machine with opposite rotation directions.

However, the performances of the obtained asymmetric designs are strongly dependent on the operating mode, as highlighted in Table I. While their torques at their specific working point and rotation direction are very high, they perform poorly in the complementary operating mode. Because of this, it is then interesting to consider both generator and motor working points within the same optimization process to increase the multi-functionality of the optimized design.

By doing so, we obtain a symmetric geometry represented in Fig. 11a which looks more conventional and close to the reference design Fig. 6a. This design is indifferent to the operating mode: it can work well for both generator and motor modes, whatever the rotation direction, while previous asymmetric designs require changing the rotation direction to perform well in the other mode. Versatility is a characteristic of symmetric designs, as they perform identically in motor or generator mode whatever the rotation direction, see Table II. Moreover, it outperforms the reference structure Fig. 6a from a magnetic point of view because it removes the PM magnetic short circuits.

Yet, this symmetric structure cannot reach the performances of asymmetric ones for the specific application cases they were designed for.

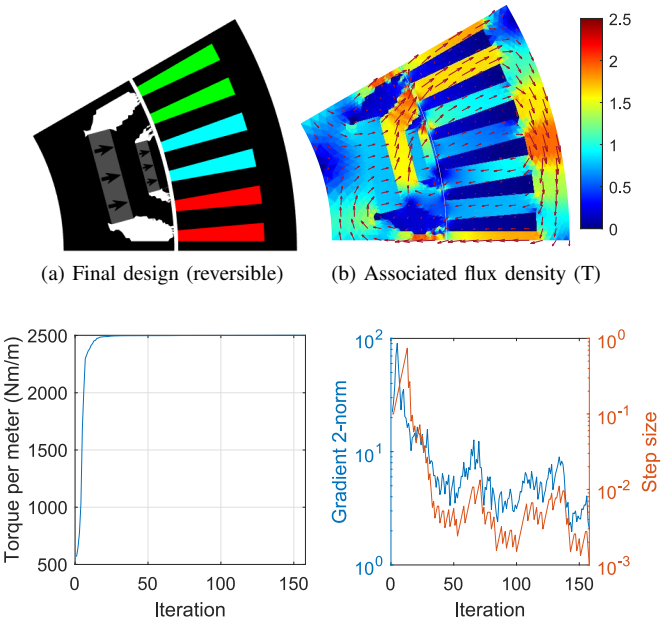

(a) Final design (reversible) (b) Associated flux density (T)

(c) Average of absolute motor and generator torques (d) Gradient norm and step size during the optimization process

Fig. 11. Optimization results for both motor and generator working points.

TABLE I
OPTIMIZATION RESULTS (TRIGONOMETRIC ROTATION DIRECTION)

Test case	Symmetry	|Torque| (mot.)	|Torque| (gen.)
Reference	yes	2169 Nm/m	2169 Nm/m
Motor	no	2554 Nm/m	1618 Nm/m
Generator	no	1611 Nm/m	2549 Nm/m
Reversible	yes	2497 Nm/m	2505 Nm/m

IV. Discussion

Asymmetrical rotors exist in the literature. The physical justification for such a design relies on the utilization ratio of the reluctant torque (due to magnetic circuit) and the hybrid torque (due to interaction between PM and current flux) [26].

As shown in Fig. 12, such a design is not a surprise because the flux distribution cannot be symmetric due to the presence of PM. Indeed, a flux analysis performed on the symmetric design (Fig. 11a) shows that:

- The flux distribution generated by the PM only – with a remanent flux density of $1\,\mathrm{T}$ – shown in Fig. 12a is symmetric.
- The flux distribution generated by the windings – with a current density of $10\,\mathrm{A/mm^2}$ and no remanent flux density – shown in Fig. 12b is also symmetric.
- These two flux distributions are both symmetric but are in quadrature. Therefore, their vector combination is asymmetric, as shown in Fig. 12c.

The unsaturated iron can be removed where the windings component and the PM component of the flux compensate for each other without reducing the performance. Moreover, by doing so, flux leakages and magnetic short circuits may also be reduced as in the circled zone shown in Fig. 12d, leading to a slight increase of the torque.

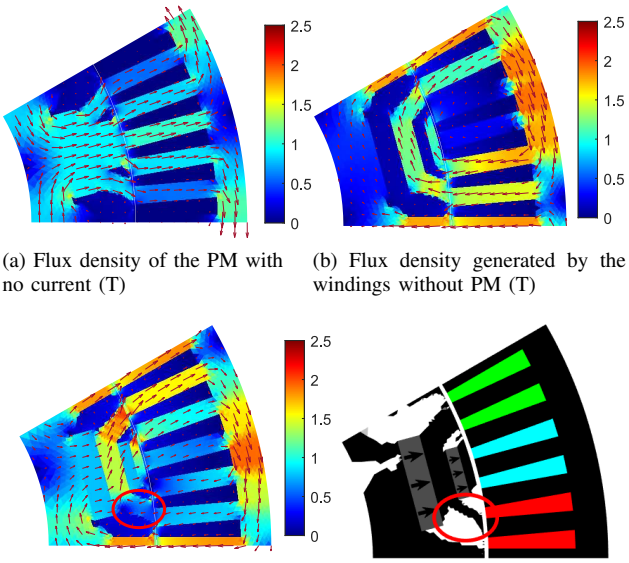

(a) Flux density of the PM with no current (T)

(b) Flux density generated by the windings without PM (T)

(c) Flux generated by both windings and PM (T)

(d) Optimized asymmetric design (motor mode)

Fig. 12. Contributions of the PM and winding flux distributions in a symmetric design (motor working point).

This analysis holds for the generator operating mode and the reverse rotation direction. It justifies the asymmetry of pure motor and pure generator rotors as well as the symmetry of the reversible structure. The optimized machine performances are summarized in Table I.

Notice that asymmetric structures can provide a slight increase of the torque ($+2\,\%$) for the specific working point for which they are optimized, but their performances are significantly decreased ($-36\,\%$) for the complementary operating mode. These characteristics are compared in Table II for all optimized designs, rotation directions, and possible operating modes, indicating that asymmetric rotor structures are more specific than symmetric ones.

TABLE II
COMPARISON OF OPTIMIZED MACHINES PERFORMANCES

Machine	Motor ↺	Generator ↺	Motor ↻	Generator ↻
Motor (Sec. III-B)	++	– –	– –	++
Generator (Sec. III-C)	– –	++	++	– –
Reversible (Sec. III-D)	+	+	+	+

V. Conclusion and Perspectives

In this paper, we presented a density-based topology optimization method. It was applied to find an optimized iron distribution within a PMSM rotor. Although atypical, we analyzed and justified the results corresponding to non-symmetrical rotor structures. These analyses suggest that asymmetric topologies could be well-suited for pure motor (gas extraction) or generator (wind turbines, avionics) applications, while symmetric designs would be a better choice for multi-function purposes (electric vehicles).

Moreover, these results show the usefulness of topology optimization methodologies in the field of electrical machine design, as they allow the conception process to be freed from the bias of designers. However, this study has also highlighted the difficulties such an approach can pose, as the designer must clearly and exhaustively define the optimization problem to avoid overspecialized results.

The effect of the rotor's asymmetry on other parameters, such as losses, torque ripple, mechanical strength, or manufacturability, were not considered and should be investigated in future works. This methodology may therefore be enriched by other physics and constraints (such as radial forces, thermic, and mechanical resistance) as well as several additional materials, including free PM placement, to address industrial problems.

References

[1] D. N. Dyck and D. A. Lowther, "Automated design of magnetic devices by optimizing material distribution," *IEEE Transactions on Magnetics*, vol. 32, no. 3 PART 2, pp. 1188–1192, 1996.

[2] S. I. Park and S. Min, "Design of magnetic actuator with nonlinear ferromagnetic materials using level-set based topology optimization," *IEEE Transactions on Magnetics*, vol. 46, no. 2, pp. 618–621, 2010.

[3] P. Gangl, S. Amstutz, and U. Langer, "Topology Optimization of Electric Motor Using Topological Derivative for Nonlinear Magnetostatics," *IEEE Transactions on Magnetics*, vol. 52, no. 3, pp. 4–7, 2016.

[4] J. S. Choi, K. Izui, and S. Nishiwaki, "Multi-material optimization of magnetic devices using an Allen-Cahn equation," *IEEE Transactions on Magnetics*, vol. 48, no. 11, pp. 3579–3582, 2012.

[5] F. Campelo, J. A. Ramírez, and H. Igarashi, "A survey of topology optimization in electromagnetics : considerations and current trends," pp. 2–47, 2010. [Online]. Available: https://www.academia.edu/2751679/A_survey_of_topology_optimization_in_electromagnetics_considerations_and_current_trends

[6] M. P. Bendsøe and N. Kikuchi, "Generating optimal topologies in structural design using a homogenization method," *Computer Methods in Applied Mechanics and Engineering*, vol. 71, pp. 197–224, 1988.

[7] J. Lee, J. H. Seo, and N. Kikuchi, "Topology optimization of switched reluctance motors for the desired torque profile," *Structural and Multidisciplinary Optimization*, vol. 42, no. 5, pp. 783–796, 2010.

[8] F. Guo and I. P. Brown, "Multi-material magneto-structural topological optimization of wound field synchronous machines," *2019 IEEE Energy Conversion Congress and Exposition, ECCE 2019*, pp. 6516–6523, 2019.
[9] F. Guo and I. P. Brown, "Simultaneous Magnetic and Structural Topology Optimization of Synchronous Reluctance Machine Rotors," *IEEE Transactions on Magnetics*, vol. 56, no. 10, 2020.
[10] E. Kuci, P. Duysinx, and C. Geuzaine, "Combination of topology optimization and Lie derivative-based shape optimization for electromechanical design," *Structural and Multidisciplinary Optimization*, vol. 59, pp. 1723–1731, 2019.
[11] T. Gauthey, P. Gangl, and M. H. Hassan, "Multi-Material Topology Optimization with Continuous Magnetization Direction for Permanent Magnet Synchronous Reluctance Motors," 2021. [Online]. Available: http://arxiv.org/abs/2107.04825
[12] O. Sigmund, "On the usefulness of non-gradient approaches in topology optimization," *Structural and Multidisciplinary Optimization*, vol. 43, no. 5, pp. 589–596, 2011.
[13] K. Svanberg, "The method of moving asymptotes—a new method for structural optimization," *International Journal for Numerical Methods in Engineering*, vol. 24, no. 2, pp. 359–373, 1987.
[14] M. P. Bendsøe and O. Sigmund, *Topology Optimization : Theory, Methods and Applications*, Springer-Verlag, Ed. Springer, 2003.
[15] M. P. Bendsøe and O. Sigmund, "Material interpolation schemes in topology optimization," *Archive of Applied Mechanics*, vol. 69, no. 9-10, pp. 635–654, 1999.
[16] O. Sigmund and J. Petersson, "Numerical instabilities in topology optimization: A survey on procedures dealing with checkerboards, mesh-dependencies and local minima," *Structural Optimization*, vol. 16, no. 1, pp. 68–75, 1998.
[17] E. Kuci, F. Henrotte, P. Duysinx, and C. Geuzaine, "Design sensitivity analysis for shape optimization based on the Lie derivative," *Computer Methods in Applied Mechanics and Engineering*, vol. 317, pp. 702–722, 2017.
[18] J. S. Choi and J. Yoo, "Structural optimization of ferromagnetic materials based on the magnetic reluctivity for magnetic field problems," *Computer Methods in Applied Mechanics and Engineering*, vol. 197, no. 49-50, pp. 4193–4206, 2008.
[19] P. Dular and C. Geuzaine, "Getdp: a general environment for the treatment of discrete problems," 1997. [Online]. Available: http://geuz.org/getdp/
[20] A. Arkkio, "Analysis of Induction Motors Based on the Numerical Solution of the Magnetic Field and Circuit Equations." Ph.D. dissertation, Helsinki University of Technology, 1987.
[21] X. Shi, Y. Le Menach, J. P. Ducreux, and F. Piriou, "Comparison of slip surface and moving band techniques for modelling movement in 3D with FEM," *COMPEL - The International Journal for Computation and Mathematics in Electrical and Electronic Engineering*, vol. 25, no. 1, pp. 17–30, 2006.
[22] C. Geuzaine and J. Remacle, "Gmsh: A 3-D finite element mesh generator with built-in pre- and post-processing facilities," *International Journal for Numerical Methods in Engineering*, vol. 79, no. May, pp. 1309–1331, 2009. [Online]. Available: http://onlinelibrary.wiley.com/doi/10.1002/nme.3279/full
[23] J. Nocedal and S. J. Wright, *Numerical optimization*, P. Glynn and S. M. Robinson, Eds. Springer, 2006.
[24] D. Staton and J. Goss, "Open Source Electric Motor Models for Comercial EV&Hybrid Traction Motors," in *CWIEME*, Berlin, 2017, pp. 46–59.
[25] A. N. A. Hermann, N. Mijatovic, and M. L. Henriksen, "Topology optimisation of PMSM rotor for pump application," *Proceedings - 2016 22nd International Conference on Electrical Machines, ICEM 2016*, pp. 2119–2125, 2016.
[26] Y. Xiao, Z. Zhu, G. Jewell, J. Chen, D. Wu, and L. Gong, "A Novel Asymmetric Rotor Interior Permanent Magnet Machine with Hybrid-Layer Permanent Magnets," *IEEE Transactions on Industry Applications*, vol. 57, no. 6, pp. 5993–6006, 2021.

VI. Biographies

Théodore Cherrière received his M.Sc. degree in electrical engineering from the Paris-Saclay University and École Normale Supérieure Paris - Saclay – France in 2020. He is currently a Ph.D. candidate in the SATIE laboratory from the same university. His research interests include electromagnetics computing, multiphysics simulations, and topology optimization.

Sami Hlioui is full professor at CY Cergy-Paris University – France and researcher in the SATIE laboratory of the École Normale Supérieure Paris - Saclay – France. He obtained his M.Sc. degree in electrical engineering from the ENS Cachan – France, his Ph.D. degree in electrical power engineering from the University of Technology of Belfort-Montbeliard – France (UTBM) in 2008, and his H.D.R (accreditation to supervise research) in 2018 from École Normale Supérieure Paris – Saclay - France. His main research interest is the multidisciplinary modeling of electromagnetic actuators (electromagnetic modeling in low (0..10kHz) and high (100kHz..10MHz) frequency domain, thermal and mechanical models) and the optimal design of these actuators for embedded applications (automotive and airplane applications). He currently participates in several research programs and supervises different Ph.D. thesis.

Luc Laurent is Assistant Professor in structural mechanics at the Conservatoire national des arts et métiers in Paris. He does his research in the Structural Mechanics and Coupled Systems Laboratory (LMSSC). He obtained his M.Sc. degree in computational and structural mechanics and his Ph.D. in mechanical engineering from the École Normale Supérieure de Cachan respectively in 2010 and 2013. His main research topics are optimization based on Gaussian Process, reduced-order modeling, uncertainty propagation applied to vibro-acoustics and structural dynamics problems.

François Louf received the Ph.D. degree in mechanical engineering from the École Normale Supérieure de Cachan, (Cachan, France), in 2003. He received the HDR from the École Normale Supérieure Paris-Saclay, (Cachan - France), in 2017. He was an Assistant Professor at Paris X Nanterre, Nanterre, France, in 2003. Since 2005, he has been with the LMT laboratory, ENS Paris-Saclay (now known as LMPS laboratory). His main research interests are model validation, uncertainties in finite-element models, and model updating with real-time constraints.

Hamid Ben Ahmed received the Ph.D. degree from the Paris VI University in 1994 and HDR degree from the Paris XI University in 2006. Since 1997, he has been an Assistant Professor in the Mechatronics Department of École Normale Supérieure de Rennes, France, and the head of this Departement since 2018. His research interests include the life cycle analysis, design, modeling, and optimization of novel topologies of electromagnetic machines. His research also concerns the optimization methodologies of renewable energy systems and smart grids.

Mohamed Gabsi received his Ph.D. degree in electrical engineering from University of Paris-VI in 1987 and his HDR in 1999 from University of Paris-XI (Orsay, France). Since 1990, he has been working in the electrical machine team of SATIE laboratory, where he is currently a full professor and researcher. His research interests include SRM, vibrations and acoustic noise, and PM machines.